Low-yttria doped zirconia: Bridging the gap between strong and tough ceramics

M. Imariouane, M. Saadaoui, G. Denis, Helen Reveron, Jérôme Chevalier

Low-yttria doped zirconia: bridging the gap between strong and tough ceramics

M. Imariouane[1], M. Saâdaoui[1], G. Denis[2], H. Reveron[2], J. Chevalier [2]

[1]Université Mohammed V de Rabat, EMI, Avenue Ibn Sina, 10000 Rabat, Morocco

[2]Université de Lyon, INSA de Lyon, Université Claude Bernard Lyon 1, CNRS, MATEIS, UMR5510, Villeurbanne, France

Abstract

This work deals with the mechanical behavior of a zirconia ceramic doped with 1.5 mol% of yttria, recently developed by Tosoh (Japan). The results show that this material offers an attractive combination of strength (1 GPa) and toughness (8.5 MPa$\sqrt{m}$), near the optimum between a brittle and ductile behavior. This is attributed to the crack shielding effect of phase transformation toughening mechanism, which is here more developed compared to conventional 3Y-TZP. Moreover, a relatively high Weibull modulus of 16 and a significant crack growth resistance were observed. It was also shown that the obtained slow crack growth threshold (5.6 MPa$\sqrt{m}$) is roughly twice that of 3Y-TZP. A qualitative investigation showed that phase transformation also occurred during impact testing, which is promising for the impact resistance of this material. Although tough and strong, the material exhibits a high resistance to aging compared to standard 3Y-TZP.

Keywords: 1.5Y-TZP, fracture toughness, flexural strength, crack growth resistance, phase transformation.

1. Introduction

Yttria-Tetragonal Zirconia Polycrystals (Y-TZP) are widely used for structural engineering including biomedical applications, due to their biocompatibility and interesting mechanical properties. In these ceramic materials, tetragonal metastable state of zirconia is retained at room temperature by the addition of yttria (Y_2O_3) typically in the range of 2.5 to 3.5 mol% [1, 2]. Under external applied stresses, they may present a stress-induced tetragonal-to-monoclinic (t-m) transformation, accompanied by volume expansion inducing compressive stresses, which hinder crack propagation and thus contribute to their toughening [1- 3].

It is commonly recognized that the strength and the toughness of Y-TZP materials depend on the stabilizer content and the grain size of the material. However, the conditions that maximize

the strength and the toughness are not usually coincident. Submicron 3 mol% yttria-stabilized zirconia (3Y-TZP) exhibits the highest strength (which can be higher than 1 GPa) for single-phase oxide ceramics, but only moderate fracture toughness (4 - 6 MPa$\sqrt{m}$) [4 - 6]. Increasing the grain size increases the transformability and thus the fracture toughness [7 - 12]. Reduction of the stabilizer amount can also be used to increase the t–m transformation ability of Y-TZP, resulting in an increase of the toughness [10, 13, 14]. For example, Trunec et al [15] showed that decreasing the yttria content to 1.5 mol% resulted in an increase of the toughness to 7.9 MPa$\sqrt{m}$ for a nanocrystalline zirconia with a grain size of 85 nm. However, only a few works have been published on mechanical properties of Y-TZP with less than 3 mol% of the yttria-stabilizer (Tab. 1). For most of them, strength values are lacking or determined on a very limited number of samples. Moreover, the toughness was often determined by the indentation fracture method, known to overestimate the toughness of transformable zirconia ceramics. As an example, for 1.5Y-TZP, Trunec et al. [15] obtained a toughness value of 15.5 MPa$\sqrt{m}$ by the indentation fracture method while the same authors obtained only 7.9 MPa$\sqrt{m}$ when the toughness was measured by the chevron notched beam method. Kern et al. [16] reported high toughness values (10.5 – 12.5 MPa$\sqrt{m}$) for Y-TZP materials obtained from stabilizer-coated powders with stabilizer contents between 2.6 and 2.85 % mol, sintered at 1350°C. The authors outlined that the toughness in these materials is not only related to stabilizer content and grain size, but to a complex process involving the partitioning of yttria, grain growth and residual stresses.

Strength and toughness are linked in ceramic materials. In general, it is obviously considered that the higher the toughness, the higher the strength, following the well-known equation:

$$\sigma_f = \frac{K_{IC}}{\sqrt{\pi a}} \qquad (1)$$

where the strength, σ_f, increases with the fracture toughness, K_{IC}, and where a is the defect size (related to process quality).

However, Eq. 1 is not fully valid in zirconia-based ceramics, especially when transformation toughening becomes extensive. Swain et al [7, 17] indeed distinguished two regimes for zirconia ceramics: Low toughness values correspond to the flaw limited strength regime, well-described by Eq. 1. Above a certain toughness (about 8 MPa$\sqrt{m}$), an inverse relation is observed, corresponding to the transformation-limited strength regime, generally accompanied by an R-curve behavior (increase of the crack growth resistance with crack extension), where the strength is here limited by the critical stress of t-m phase transformation that occurs before

failure. In other words, above a certain toughness, the maximum sustainable stress is the critical stress for transformation, $\sigma_c^{t\text{-}m}$, which decreases with toughness (higher transformability).

Over the last two decades, studies focused on strategies to obtain a better balance between strength and toughness in zirconia based ceramics. Attractive combination of strength and toughness was obtained for TZP materials co-stabilized with yttria and neodymia [18]. Casellas et al. [19] produced materials with a mixed phase assemblage of TZP and PSZ (partially stabilized zirconia consisting of tetragonal precipitates embedded in a cubic matrix), that allowed increasing the transformability with limited decrease in strength compared to the 2.5Y-TZP used as a base. Another approach consists of developing Ce-TZP-based composites [20 - 22] with ductile behavior due to high amount of transformation. Therefore, more than increasing strength or toughness 'only', it is important to obtain a balance between these two properties, best being at the peak of the σ_f-K_{IC} curve, where the brittle strength given by Eq. 1 is equal to the critical stress for transformation. Moreover, besides a high toughness corresponding to fast loading conditions, a good resistance to SCG is also required for structural and biomedical applications. In particular, the stress intensity threshold K_{I0}, below which there is no crack propagation even at low rate, is a crucial parameter which characterizes the safety range for the material intended for long-term clinical use.

Recently, Tosoh Company (Japan) developed a new Y-TZP zirconia, Zgaia 1.5Y-HT, entirely retained as the tetragonal phase with low concentration of stabilizer, i.e. 1.5 mol% Y_2O_3, and addition of 0.25 mass% Al_2O_3 [23]. In this work, a systematic investigation of the mechanical behavior of this material was performed, including determination of the intrinsic toughness, the flexural strength under uniaxial and biaxial loading, the crack growth resistance curve (R-curve) and SCG resistance. Low-temperature degradation (LTD), or aging, considered to be a key issue for the safe application of Y-TZP ceramics [24] and the impact resistance, which is rarely explored for ceramic materials, were also investigated.

2. Material and Methods

2.1. Material and preliminary characterization

The material used in this study was a 1.5 mol% Yttria stabilized zirconia (1.5Y-TZP), provided by Tosoh in the form of sintered samples. Sintering was performed at relatively low temperature, at 1350°C for 2 hours, thanks in part to the addition of 0.25 mass% Al_2O_3. Three types of samples were provided: rectangular bars with polished edges (4 mm × 3 mm× 42 mm) for four points bending (4PB) tests, plates (20 mm × 2 mm× 42 mm) for Double Torsion (DT)

tests and disks (diameter of 18 mm and thickness of 1 mm) for biaxial strength measurements and impact tests.

A preliminary characterization of the material was performed including the measurements of the Vickers hardness, the density by the Archimedes' method and the Young modulus by the resonance vibration method (Grindo-Sonic tester). The microstructure was investigated by Scanning Electron Microscopy (SEM; Zeiss SUPRA VP55, Switzerland) observations of polished and thermally etched samples (1250°C, 20 min) to reveal the grain boundaries, and the grain size was evaluated by the linear-intercept method applying a multiplying factor of 1.56 to account for the 2D to 3D correction [33].

2.2. Phase composition and transformability

To determine the phase composition and to investigate the transformability of the material, X-Ray Diffraction (XRD) analysis was performed (D8 Advance Bruker AXS diffractometer (Billerica, USA, CuKα1) in the angular domain 2θ between 27 and 32°. The mass fraction of the monoclinic phase (X_m) was calculated according to the following expression [34]:

$$X_m = \frac{l_m(\bar{1}11) + l_m(111)}{l_m(\bar{1}11)+l_m(111)+l_t(101)} \quad (2)$$

where $I_m\ (hkl)$ denotes the area of the peak generated by the hkl plane in the monoclinic (m) or the tetragonal phase (t).

The volume fraction was then calculated according to [35]:

$$V_m = \frac{1.311X_m}{1+0.311X_m} \quad (3)$$

The phase transformation zones induced during the different mechanical tests were characterized by optical (ZEISS Axiophot and Hirox RH-2000) and 3D confocal Microscopy using a S-Neox (Sensofar, Terrassa, Spain) 3D non-contact optical profiler machine, which combines confocal and interferometry techniques with lateral resolution of 0.26 µm, the acquired data were processed using Mountains Map Universal software ® (Digital Surf, Besançon, France).

2.3. Flexural strength measurements

Strength measurements were conducted on 30 rectangular bars in 4PB tests, with outer and inner spans respectively of 35 and 10 mm and the results were statically analyzed using Weibull and Normal statistical distributions. Three balls on three balls (3B3B) biaxial bending tests were also performed on 10 samples, using the protocol described in [36]. The sample was supported by 3 balls positioned on a circle of 8 mm radius and the load was applied by three balls positioned on a circle of 4 mm radius. For both tests, the experiments were performed on polished (down to 1 µm) samples using a universal testing machine (Instron 8500). The cross-head speed was set at 1 mm/min until failure, to avoid SCG effects.

2.4. Toughness and R-curve measurements

The fracture toughness, K_{IC}, and the crack growth resistance curve (R-curve) were determined by the single-edge V-notched beam (SEVNB) method [37] on rectangular bars with one side polished down to 1 µm finish in order to facilitate crack growth observations. The tests were conducted on a universal testing machine (Instron 8500). For K_{IC} measurements, a first notch was cut using a thin diamond saw and then tapered by ultrashort pulsed laser ablation notching to obtain a relative total notch depth of 0.25 and a notch root radius of about 1.5 µm. The samples were loaded on a 4PB device (10-35 mm spans) at a cross-head speed of 1 mm/min. For the R-curve determination, the saw-cut notches were further sharpened with a fine razor blade sprinkled with a diamond paste of 1 µm and the final relative notch depth was of 0.4. The samples were annealed at 1200°C for 20 min (with heating and cooling rates of 10°C/min) to eliminate the machining residual stresses, then loaded in three points bending (3PB) with a span of 35 mm and a cross-head speed of 0.005 mm/min to allow stable crack growth. The R-curve was determined from the recorded load-displacement curve, in terms of the stress intensity factor, K_R, plotted versus the crack extension, Δa, determined by a compliance formula [38] corrected by an empirical factor, adjusted so that the final calculated crack length corresponded to the measured value at the end of the test. K_R was calculated from the recorded load and the corresponding crack length using the geometrical factor reported in [39].

2.5. Double torsion tests

The DT method was used to investigate the SCG behavior and to determine the overall crack propagation rate versus stress intensity factor (V-K_I) curve. The tests were conducted as described in [40]. A notch of length $a_0 \approx 10$ mm and width 0.3 mm was machined with a diamond blade and two Vickers indentations were then introduced ahead of the notch tip in

order to initiate a small crack. Subsequent pre-cracking was performed by slowly loading the specimens at a cross-head speed of 0.01 mm/min to introduce an initial sharp crack with a length, a_i, of 12–15 mm, so that the crack tip was far enough from the indentations.

The V-K_I curve was determined using relaxation and constant loading tests as detailed in [40, 41]. Relaxation tests allow determination of V-K_I curves for velocities ranging between 10^{-7} to 10^{-2} m/s, while constant loading tests enable measurement of crack velocities down to 10^{-11}m/s and estimate the threshold stress intensity factor below which no crack propagation occurs [42]. The value of this threshold, K_{I0}, is actually of major importance when considering avoiding any delayed failure in service. In the relaxation tests, the pre-cracked specimens were loaded at a constant rate of 0.4 mm/min to a certain load, and then the crosshead was stopped at a constant displacement. The relaxation curve (load versus time) and the crack length, a, determined from a compliance calibration curve, were used to calculate the applied stress intensity factor, K_I, using the following expression [40]:

$$K_I = P\frac{W_m}{T^2}\left(\frac{3(1+\nu)}{W\psi}\right)^{\frac{1}{2}}\left(\frac{a}{a_0}\right)^{\frac{6}{32}} \qquad (4)$$

where P is the applied load, W_m the span length, T and W the sample thickness and width, ν the Poisson ratio (taken equal to 0.25), ψ a calibration factor [43]. a and a_0 represent the crack and notch length respectively. The crack growth rate, V, was calculated as follows [44]:

$$V = -\frac{P_f}{P^2}\left(a_f + \frac{D}{B}\right)\frac{dP}{dt} \qquad (5)$$

where P_f is the final load, a_f the final crack length, D and B are constants obtained from the compliance calibration curve, and dP/dt the relaxation slope at a given time.

For the constant-loading tests, the DT specimens were subjected to different constant loads for a prescribed duration, Δt, and the crack increment, Δa, was measured via reflected-light optical microscopy, with a resolution of 2 µm. The ratio of Δa to Δt gives directly the crack growth rate, V, related to the applied stress intensity factor.

To evaluate the fracture toughness by DT, some samples were loaded to fracture at a high displacement rate of 5 mm/min and K_{IC} was calculated by Eq. 4 using the maximum load and the measured crack length before testing.

2.6. Impact resistance

Evaluation of the impact resistance was performed through drop weight tests performed on disk-shaped samples using a device developed in the laboratory. During the test, the sample was supported by three balls located in a circle of 8 mm radius, as in the 3B3B biaxial tests. A tungsten carbide ball of 26.5 g weight and 15 mm diameter was dropped on the center of the disk from a height that was increased in small increments from an initial height set at 30 cm, until fracture occurred. The impact energy, E_{imp}, was calculated considering only the potential energy, i.e. and ignoring the loss due to air resistance, as follows:

$$E_{imp} = mgH \quad (6)$$

where m is the mass of the tungsten carbide drop ball (26.5 g) and H is the drop height.

2.7. Low temperature degradation

To investigate the susceptibility to LTD, accelerated hydrothermal aging tests were carried out by exposing the material to a saturated water vapor atmosphere in a stainless-steel autoclave at 134°C and under a pressure of 2 bar, according to ISO 13356 standard. In the case of zirconia, it has been shown that 1 h of this treatment corresponds roughly to 4 years at the body temperature [45]. It is therefore a good indication of the resistance to aging of a given yttria-doped zirconia, which would be used for biomedical applications. The LTD was quantified by following the amount of tetragonal to monoclinic phase transformation on polished surfaces as function of aging time. The volume fraction of the monoclinic content was determined by XRD as described in section 2.2.

3. Results

3.1. Microstructure and preliminary characterization

Figure 1 shows SEM micrographs of polished and thermal etched surfaces, from which an average grain size of 440 ±70 nm was obtained. The measured density is 6.08 ± 0.01 g/cm^3, the Young's modulus and the Vickers hardness are respectively 218 ± 0.4 GPa and 11.8 ± 0.2 GPa, in the typical range for Y-TZP ceramics. The volume fraction of the monoclinic phase measured by XRD on the polished surface was about 5 ± 2%.

3.2. Flexural strength

Figure 2 shows examples of the loading curves during uniaxial 4PB and biaxial 3B3B tests. For both configurations, no evident deviation from linearity was observed until fracture, and the average strength was respectively 995 ± 77 MPa and 1320 ± 160 MPa for 4PB and 3B3B

samples. Figure 3 shows the tensile side of both types of samples, observed by optical microscopy in Nomarski contrast. In the biaxial configuration, transformed bands located at the center of the sample (where the stress is maximum) appeared at an applied stress of 800 MPa, then multiplied and propagated in the form of a star-shaped zone. In the 4PB configuration, narrow parallel transformation bands were generated on the tensile side, just before failure (at around 950-1000 MPa). The 4PB strength data were analyzed according to a Weibull distribution [46]. Unbiased values of the Weibull modulus, m, and the characteristic strength, σ_0 (the stress corresponding to 63% fracture probability), with their 90% confidence intervals, were calculated following [47]. The obtained values are respectively 15 [11-20] and 1062 [1037-1087] MPa. The Weibull modulus is similar to that reported for 3Y-TZP materials with equivalent grain size [48] for which however, lower strength values of 914 MPa and 627 MPa were obtained respectively from piston on three balls [48] and 3PB [14] tests. The failure distribution was also analyzed according to a simple Normal function and the obtained probability fit was equivalent to that of the Weibull analysis (Figure 4).

3.3. Toughness and R-curve behavior

The fracture toughness obtained from SEVNB tests is 8.5 ± 0.2 MPa$\sqrt{m}$ and no difference was observed between the as-received and annealed samples. As shown in Figure 5, the crack-growth resistance, K_R, starts from an initial value, K_{R0}, of 7 MPa$\sqrt{m}$ and increased over a crack extension Δa^* about 100 µm, to a steady state value (plateau value) of 8 MPa$\sqrt{m}$. It is to note that as the tests were performed at a very low speed (0.005 mm/min) the R-curve effect may be limited by SCG as reported in [9, 49], where K_R was reduced by 30 to 40 % in air compared to an inert environment.

3.4. V-K_I curves

The V-K_I curve is shown in Figure 6, where the results of a 3Y-TZP [40] and a highly transformable 10Ce-TZP/$MgAl_2O_4$ composite [50] tested following the same methodology are also plotted for comparison. The indicated fracture toughness (K_{IC} = 10.6 MPa$\sqrt{m}$) corresponds to the value measured separately from fast loading tests. The determined V-K_I curve shows the three typical stages corresponding to stress induced corrosion by water molecules, known to occur in oxide ceramics [42, 51 - 54] and a threshold, K_{I0}, below which no detectable crack propagation occurs.

Stage I, which correspond to the low-velocity regime, can be well fitted by a power-law [55]:

$$V = A.K_I^{\,n} \qquad (7)$$

where A and n are parameters depending on the material, temperature and environment.

The value of stress corrosion susceptibility coefficient n, is 30, which is equivalent to that generally reported for zirconia ceramics [22]. The threshold, determined from the stress intensity factor below which no detectable crack growth occurs is 5.1 MPa$\sqrt{m}$. Compared to 3Y-TZP for which the threshold is about 3.5 MPa$\sqrt{m}$ [42], the V-K_I curve is shifted to higher K_I values, with a higher threshold.

3.5. Impact resistance under drop weight test

Optical observations of the tensile side of unbroken samples revealed that t-m phase transformation occurred during the impact testing as shown in Figure 7. The impact-induced transformation zone has a star-shape geometry, with a circular central region and radial bands running towards the edge of the disk. The size of the transformation zone was evaluated considering the transformed area within a circle corresponding to the effective surface, considered equivalent to that of biaxial piston-on-three balls test [56]. The transformation zone size increases with the impact energy. 3D confocal microscopy allowed quantitative analysis of the topography of impacted samples. The volume increase associated to the transformation was evidenced by circular dome shaped zones (Figure 8) and it is noted that the effect of the impact extended to the entire sample, as evidenced by the absence of flat area on the images. From radial roughness profiles (Figure 8) it can be seen that the maximum height of the transformation zone increased from 0.5 µm to 1.5 µm as the drop height (h) was increased from 30 cm to 45 cm. The fracture occurred at a drop height of h=50 cm and it was initiated along transformation bands as also observed for biaxial tests.

3.6. Low temperature degradation

Figure 9 shows the evolution of the monoclinic content ΔV_m (= $V_m(t) - V(t=0)$) with aging time for the studied 1.5Y-TZP and for a standard 3Y-TZP [40], also tested for comparison. Overall, the aging kinetics of the present material, although presenting less nominal yttria content, is slower than for the benchmark 3Y-TZP. After 50 hours in autoclave, ΔV_m reached 70% for 3Y-TZP while it was only of 45% for 1.5Y-TZP.

4. Discussion

4.1. Effect of the transformability on mechanical behavior

Although no evidence of macroscopic plasticity on the loading curves, the occurrence of phase transformation during flexural tests (Figure 3) is an indicator of the very beginning of transformation-induced microscopic plasticity. Moreover, the difference of transformability

features between biaxial and uniaxial tests is analogous to that already reported for ceria-doped zirconia (Ce-TZP) composites with transformation-induced plasticity [6, 56- 58], but with less consequence on the measured strengths. For ductile Ce-TZP composites [56], the biaxial strength reached up to 2.5 times the uniaxial one and it was concluded that calculated stresses for biaxial tests based on elastic assumptions were not correct as the applied stress is shielded by the transformation. For the present 1.5Y-TZP, the difference between the biaxial and the uniaxial strengths is 30%, which is similar to that reported for a 3Y-TZP material [6] with a brittle behavior, well described by (Eq. 1) between toughness and strength, and for which no transformation occurred before failure.

The measured SEVNB toughness value (8.5 MPa$\sqrt{m}$) is very high for Y-TZP ceramics. For comparison, lower toughness values of 5.9 and 4.7 MPa$\sqrt{m}$ were reported respectively for 2Y-TZP [29] and 3Y-TZP [48] with grain sizes similar to that of the studied material and 7.9 MPa$\sqrt{m}$ was obtained for a nanocrystalline zirconia stabilized with 1.5 mol.% Y_2O_3 [15]. For zirconia stabilized with less than 3 mol.% Y_2O_3, higher values in the range of 13 to 17 MPa$\sqrt{m}$ were obtained only by the indentation fracture method [13, 15, 25], known to overestimate the fracture toughness of transformable zirconia materials. It is to note that for the present 1.5Y-TZP, the DT method resulted in a higher toughness (10.6 ± 0.2 MPa$\sqrt{m}$) compared to the SEVNB method. This can be attributed to the observed rising R-curve behavior. Taking into account the R-curve effect and the influence of SCG, the fracture toughness value obtained by the SEVNB tests is more realistic as in this configuration, the fracture corresponds to small cracks, whereas the DT value obtained for long cracks corresponds to the plateau value.

The high toughness and the crack growth resistance observed in the studied material can be attributed to the extrinsic phase transformation toughening that shields the crack tip from the applied stress intensity [1, 59]. This effect is described by a stress intensity change, K_{sh} (Eq. 8), between the applied stress intensity factor, K_R, and the stress intensity factor at the crack tip, K_{R0}, which is assumed to be equal to the intrinsic toughness of the material.

$$K_R = K_{R0} + K_{sh}(\Delta a) \qquad (8)$$

To induce crack growth, the applied stress intensity factor has to be increased to overcome the shielding contribution that increases with crack extension, Δa. Thus, the crack growth resistance increases until a steady-state transformation zone is developed at a crack extension, Δa^*, corresponding to the plateau value (Figure 5). The shielding contribution can be estimated according to McMeeking and Evans model [59] as follows:

$$K_{sh} = \frac{0.22 E V_m e^T \sqrt{h}}{1-\nu} \quad (9)$$

where e^T is the dilatation strain associated to the transformation, V_m the volume fraction of transformed phase within the transformation zone, ν the Poisson ratio, and h the width of the transformation zone from the crack surface (i.e. the half-height of the zone).

The level of crack tip shielding is thus related to the volume fraction of transformable phase and the transformation zone size that increases with the phase transformability [60]. Evidence of tetragonal to monoclinic phase transformation as the active toughening mechanism in the studied material is provided from XRD analysis of polished (V_m=5$\pm$ 2%) and fractured surfaces (V_m=80$\pm$ 5%) as shown in Figure 10. Moreover, an uplift around the crack, due to the volume increase induced by the transformation was clearly detected by 3D confocal observation in a fully propagated crack during SEVNB test (Figure 11), and the measured value of the transformation zone size, h, was of 20 µm. This is in very good agreement with the observed crack extension before the plateau of the R-curve (Δa^* ~ 100 µm), which is in the order of five times the size of the transformation zone [59]. The obtained values of V_m and h are very high for Y-TZP ceramics. V_m measured by XRD on fracture surfaces are generally less than 10% for 3Y-TZP (e.g. [61]) known to have a very small transformation zone size (< 5 µm) [9, 62, 63], which induces a steep but very limited R-curve behavior (K_{sh} ~ 0.5 MPa$\sqrt{\text{m}}$) reported only for small cracks or small samples [32, 62]. In a 2.5Y-TZP with a grain size of 300 nm, Fargas et al. [31] also observed a small R-curve effect (K_{sh} = 0.4 MPa$\sqrt{\text{m}}$), from which it can be deduced that the process zone size was less than 10 µm. Eichler et al. [9] observed that no rising R-curve occurred in air for submicrometer 2Y-TZP materials with grain sizes in the range of 150 to 500 nm, for which a process zone size of 3 to 8 µm was predicted. Although a direct comparison of the plateau values cannot be made as the R-curves depend on the testing conditions, which are different from one author to another, these results clearly highlight a strong influence of yttria content: decreasing yttria content increases the transformability of the material, thus the transformation zone size and in turns the toughness and the crack growth resistance.

The higher transformation-toughening ability of the present material can also explain its higher threshold stress intensity factor compared to conventional 3Y-TZP. The real stress intensity factor at the crack tip, K_{tip}, is lower than the applied one ($K_{tip} = K_I - K_{sh}$) and the difference corresponding to the transformation-induced shielding contribution, K_{sh} is proportional to K_I as shown in [64]:

$$K_{sh} = C_{sh} K_I \quad (10)$$

In other words, Eq.10 means that the larger the applied stress intensity factor (i.e. the stresses at the crack tip), the larger is the size of the transformation size and thus the larger the transformation-induced toughening.

If the intrinsic SCG law of the material is described by the following expression:

$$V = A_0 K_{tip}^{\ n} \qquad (11)$$

where A_0 is an intrinsic parameter and K_{tip} the net stress intensity factor at the crack tip.

Then, using Eq. 10 and 11, the resulting $V–K_I$ law can be expressed as:

$$V = A_0 (1\text{-}C_{sh})^n K_I^{\ n} \qquad (12)$$

The parameter C_{sh} increases with the material transformability, so increasing the transformation toughening capacity increases the crack shielding and thus K_I. As a consequence, the V-K_I curve is shifted towards higher stress intensity factors. The shift is more pronounced for the 10Ce-TZP/$MgAl_2O_4$ composite (Figure 6) characterized by a higher transformability. Depending on the crack length, the rising part of R-curve could result in a higher slope of the V-K_I curve [65]. In the present work the transformation toughening mechanism is limited and operates over a crack length about 100 µm. The DT measurements hence correspond to steady state conditions of the R-curve and do not influence the value of the n exponent obtained for 3Y-TZP characterized by a flat R-curve behavior.

The influence of the transformation toughening is confirmed by the normalized V-K_I/K_{IC} diagram (Figure 12), where the SCG curves are normalized to the fracture toughness. A master curve is obtained, which means that the crack growth mechanism is basically the same for the three materials and that the propagation occurred through the same zirconia bonds (Zr-O-Zr) [52]. Moreover, it is commonly admitted that the higher the slope in the normalized diagram (i.e. the more the K_{I0}/K_{IC} ratio is close to 1), the less sensitive the ceramic will be to the SCG. This ratio is about 0.5, which means that the crack propagation occurs when K_I reaches half of K_{IC}, and it is likely the general rule for all zirconia ceramics, as already discussed in a previous paper [64].

4.2. Strength-toughness relationship

For the present 1.5Y-TZP, the measured strengths are close to those of 3Y-TZP for both uniaxial and biaxial loading and the 4PB value is significantly higher than that of ductile Ce-TZP composites with higher transformability (~ 600 MPa). The toughness (8.5 MPa$\sqrt{m}$) is just at (or slightly above) the transition between the two strength regimes described by Rose and Swain [66], i.e. the flaw limited strength regime (described by Eq. 1) were the strength increases

with the toughness, and the transformation-limited strength one, were the strength is limited by the critical stress of phase transformation that occurs before failure, $\sigma_c^{t\text{-}m}$. Indeed, phase transformation was observed just before fracture during 4PB tests. Also, only a limited shielding increment during crack propagation was observed from the R-curve (ΔK_{sh} ~1 MPa$\sqrt{m}$), with a dimension of the transformation zone of about 20 µm. This explains the combination of the high strength (around 1 GPa) and the relatively high toughness (more than 8 MPa$\sqrt{m}$) observed for the present material, compared to other zirconia ceramics.

Considering the concept of a process (plastic) zone as defined in [67], a chart of fracture toughness, K_{IC}, vs strength (Figure 13) can be used to discuss material's behavior in relation to the risk of brittle failure. The diagonal lines correspond to the process zone diameter, d, given by:

$$d = \frac{K_{IC}^2}{\pi \sigma_y^2} \qquad (13)$$

where σ_y is the yield stress.

Using the measured value of the intrinsic toughness and assuming that σ_y is equal to the critical transformation stress in 4PB tests, here equivalent to the fracture strength, (i.e. $\sigma_y = \sigma_c^{t\text{-}m}$ ~ 1 GPa), we obtain a process zone diameter of 23 µm which is in good agreement with the transformation zone size (h ~ 20 µm) observed experimentally. For comparison, d is only of one to few microns for 3Y-TZP zirconia and about 100 µm in ductile Ce-TZP-Alumina-Aluminates [22], in line with the transformation zone sizes in these materials. From these results, it can be concluded that the studied 1.5Y-TZP is at the transition between brittle and ductile fracture for conventional process defect sizes of tens of microns.

4.3. Aging resistance

LTD resistance of Y-TZP materials can be improved by increasing the content of yttria or decreasing the grain size [24, 68, 69], but the toughness is then compromised. In this work, the preliminary aging assessment showed that the studied 1.5Y-TZP exhibited a relatively high resistance to LTD while maintaining high values of strength and toughness. This could be explained by alumina doping that plays a crucial role for retarding the LTD, due to segregation of Al^{3+} cations at the grain boundaries [30, 70]. The relatively low sintering temperature of this material (1350°C) could also contribute to its resistance to LTD by avoiding phase partitioning and yttria depletion towards cubic grains [24]. This phenomenon occurs for materials sintered at high temperatures and consists of the formation of yttrium-rich cubic and yttrium-poor tetragonal phases. Depleted tetragonal grains are less stable to transformation and act as

preferential nucleation sites for LTD. To understand LTD mechanisms and kinetics in the studied material, a deeper investigation is necessary, especially the effect of temperature and time, as well as transmission electron microscopy to investigate yttria distribution in the grains. This will be the subject of a future paper.

5. Conclusion

The investigated 1.5Y-TZP material offers a very attractive combination of high strength and high toughness near the optimum between brittle and ductile behavior. This is due to its high transformability that also induces flaw tolerance (due to R-curve behavior) and increases the resistance to SCG, compared to conventional 3Y-TZP. Phase transformation was also observed during impact tests with an increase of the transformation zone size with the kinetic energy and further work is being undertaken to precisely characterize its effect on the impact resistance. Moreover, the material exhibited an unexpected high resistance to aging during accelerated autoclave tests at 134°C when compared to standard 3Y-TZP. This novel zirconia grade thus appears promising when a high toughness and crack resistance are necessary in demanding structural (e.g., biomedical) applications.

Acknowledgements

Thanks are due to the CLyM (Centre Lyonnais de Microscopie: www.clym.fr) for the access to the SEM. The authors would like to acknowledge Philippe Sainsot and Jérôme Cavoret (LAMCOS Laboratory- Insa Lyon) for 3D confocal experiments and Pablo Moreno and Javier Prada-Rodrigo (ALF-USAL- Universidad de Salamanca) for ultrashort laser notching. Special thanks to Tosoh Company for providing 1.5Y-TZP ceramics characterized in the present work.

References:

[1] RHJ. Hannink, PM. Kelly, BC. Muddle, Transformation toughening in zirconia containing ceramics, J. Am. Ceram. Soc. 83 (2000) 461-487.

[2] J. Chevalier, A. Liens, H. Reveron, F. Zhang, P. Reynaud, T. Douillard, L. Preiss, V. Sergo, V. Lughi, M. Swain, N. Courtois, Fourty years after the promise of « ceramic steel? »: zirconia-based composites with a metal-like mechanical behavior, J. Am. Ceram. Soc. 103 (2020) 1482–1513.

[3] A.G. Evans, A.H. Heuer, Review-transformation toughening in ceramics: martensitic transformations in crack-tip stress fields, J. Am. Ceram. Soc. 63 (1980) 241–248.

[4] B. Al-Amleh, K. Lyons, MV. Swain. Clinical trials in zirconia: a systematic review. J. Oral Rehabil. 37 (2010) 641-652.

[5] M. Turon-Vinas, M. Anglada, Fracture toughness of zirconia from a shallow notch produced by ultra-short pulsed laser ablation, J. Eur. Ceram. Soc. 34 (2014) 3865-3870.

[6] I. Touaiher, M. Saadaoui, J. Chevalier, L. Preiss, H. Reveron, Fracture behavior of Ce TZP/Alumina/Aluminate composites with different amounts of transformation toughening. Influence of the testing methods, J. Eur. Ceram. Soc. 38 (2017) 1778-1789. https://doi.org/10.1016/j.jeurceramsoc.2017.09.052.

[7] M. V. Swain, Grain Size Dependence of Toughness and Transformability of 2 mol% Y-TZP Ceramics, J. Mater. Sci. Lett., 5, (1986) 1159–61.

[8] L. Ruiz, MJ. Readey, Effect of heat-treatment on grain size phase assemblage, and mechanical properties of 3 mol% Y-TZP. J. Am. Ceram. Soc. 79 (1996) 2331–2340.

[9] J. Eichler, M. Hoffman, U. Eisele, J. Rödel, R-curve behaviour of 2Y-TZP with submicron grain size, J. Eur. Ceram. Soc. 26 (16) (2006) 3575–3582.

[10] B. Basu. Toughening of yttria-stabilised tetragonal zirconia ceramics. Int. Mater. Rev. 50, (2005) 239–256. doi:10.1179/174328005X41113

[11] M. Trunec, K. Maca, Z. Shen, Warm pressing of zirconia nanoparticles by the spark plasma sintering technique, Scr. Mater. 59 (2008) 23–26.

[12] M. Xue, S. Liu, X. Wang, and K. Jiang, “High fracture toughness of 3Y-TZP ceramic over a wide sintering range,” Mater. Chem. Phys. vol. 244, (2020) p. 122693.

[13] O. Vasylkiv, Y. Sakka, V.V. Skorokhod, Low-Temperature Processing and Mechanical Properties of Zirconia and Zirconia-Alumina Nanoceramics. J. Am. Ceram. Soc. 86 (2003) 299–304.

[14] J. Cui, Z. Gong, M. Lv, P. Rao, Determination of fracture toughness of Y-TZP ceramics, Ceram. Int. 43 (2017) 16319-16322. http://dx.doi.org/10.1016/j.ceramint.2017.09.004.

[15] M. Trunec, Z. Chlup, Higher fracture toughness of tetragonal zirconia ceramics through nanocrystalline structure, Scripta Mater. 61 (2009) 56–59.

[16] F. Kern, H. Strumberger, R. Gadow, Effects of stabilizer content and sintering conditions on Y-TZP ceramics made from stabilizer coated nanopowders, J. Ceram. Sci. Technol. 8 (2018) 7–18.

[17] M. Swain. Inelastic deformation of Mg-PSZ and its significance for strength-toughness relationship of zirconia toughened ceramics. Acta Metall., vol. 33, no 11, (1985) 2083–2091.

[18] F. Kern, R. Gadow, Alumina toughened zirconia from yttria coated powders, J. Eur. Ceram. Soc. 32 (15) (2012) 3911-3918.

[19] D. Casellas, A. Feder, L. Llanes, M. Anglada, Fracture toughness and mechanical strength of Y-TZP/PSZ ceramics, Scr. Mater. 45 (2001) 213–20.

[20] P. Palmero, M. Fornabaio, L. Montanaro, H. Reveron, C. Esnouf, J. Chevalier, Towards long lasting zirconia-based composites for dental implants, Part I: innovative synthesis, microstructural characterization and in vitro stability. Biomaterials. 50 (2015) 38–46.

[21] H. Reveron, M. Fornabaio, P. Palmero, T. Furderer, E. Adolfsson, V. Lughi, et al., Towards long lasting zirconia-based composites for dental implants: Transformation induced plasticity and its consequence on ceramic reliability, Acta Biomater. 48 (2017) 423–32.

[22] J. Chevalier, A. Liens, H. Reveron, F. Zhang, P. Reynaud, T. Douillard et al. Forty years after the promise of «ceramic steel?»: Zirconia-based composites with a metal-like mechanical behavior, J. Am. Ceram. Soc. 103 (2019) 1482-1513. https://doi.org/10.1111/jace.16903

[23] TOSOH, "Technical Data Sheet Zgaia™ 1.5Y-HT," Version 2.1, December 2021.

[24] J. Chevalier, L. Gremillard, AV. Virkar, et al. The tetragonal-monoclinic transformation in zirconia: lessons learned and future trends, J. Am. Ceram. Soc. 92 (2009) 1901-1920.

[25] A. Bravo-Leon, Y. Morikawa, M. Kawahara, M.J. Mayo, Fracture toughness of nanocrystalline tetragonal zirconia with low yttria content, Acta Mater. 50 (18) (2002) 4555–4562.

[26] K. Matsui, K. Hosoi, B. Feng, H. Yoshida, Y. Ikuhara, Ultrahigh toughness polycrystalline ceramics without fading of strength, arXiv:2112.14372 [cond-mat.mtrl-sci], 2021. https://doi.org/10.48550/arXiv.2112.14372.

[27] T. Masaki, Mechanical properties of toughened ZrO2-Y2O3 Ceramics, J. Am. Ceram. Soc. 69 (1986) 638-640.

[28] N. Gupta, P. Mallik, B. Basu, Y-TZP ceramics with optimized toughness: new results, J. Alloys Compd, 379 (2004) 228–232.

[29] B. Basu, J. Vleugels and O. Van Der Biest, Y-TZP ceramics with tailored toughness, Key Eng. Mater. Vols. 206-213 (2002) 1185-1188.

[30] F. Zhang, K. Vanmeensel, M. Inokoshi, M. Batuk, J. Hadermann, B. Van Meerbeek, I. Naert, J. Vleugels, Critical influence of alumina content on the low temperature degradation of 2–3 mol% yttria-stabilized TZP for dental restorations, J. Eur. Ceram. Soc. 35 (2015) 741–750.

[31] G. Fargas Ribas, D. Casellas Padró, L.M. Llanes Pitarch, M. Anglada Gomila, Thermal shock resistance of Y-TZP with Palmqvist indentation cracks, J. Eur. Ceram. Soc. 23 (2003) 107–114. http://dx.doi.org/10.1016/S0955-2219(02)00065-1.

[32] D. Casellas, J. Alcalá, LM. Llanes, M. Anglada, Fracture variability and R-curve behavior in yttria-stabilized zirconia ceramics, J Mater Sci 36 (2001) 3011–25.

[33] M.I. MENDELSON, Average Grain Size in Polycrystalline Ceramics, J. Am. Ceram. Soc. 52(8) (1969) 443-446.

[34] RC. Garvie, PS. Nicholson, Phase analysis in Zirconia systems, J. Am. Ceram. Soc. 55 (1972) 303-305.

[35] H. Toraya, M. Yoshimura, S. Somiya, Calibration curve for quantitative analysis of the monoclinic tetragonal ZrO2 system by X-rays diffraction, J. Am. Ceram. Soc. 67 (1984) 1197-121.

[36] T. Fett, G. Rizzi, E. Ernst, R. Müller, R. Oberacker, A 3-balls-on-3-balls strength test for ceramic disks, J. Eur. Ceram. Soc. 27 (2007) 1–12.

[37] J. Kübler, Fracture toughness of ceramics using the sevnb method: first results of a joint VAMAS/ESIS round robin, Ceram. Eng. Sci. Proc. 20 (1999) 494-502.

[38] T. Nishida, Y. Hanaki, T. Nojima, G. Pezzotti, Measurement of rising R-curve behavior in toughened silicon nitride by stable crack propagation in bending, J. Am. Ceram. Soc. 78 (11) (1995) 3113–3116.

[39] J.E, Srawley, Wide range stress intensity factor expressions of ASTM E 399 standard fracture toughness specimens. Int.J. Fract., 12(3) (1976) 475-6.

[40] J. Chevalier, M. Saâdaoui,C. Olagnon & G. Fantozzi, Double torsion testing a 3Y-TZP Ceramic. Ceram. Int, 22 (1996) 171–77.

[41] A.G. Evans, A method for evaluating the time-dependent failure characteristics of brittle materials and its applications to polycrystalline alumina, J. Mater. Sci. 7, (1972) 1137-46.

[42] J. Chevalier, C. Olagnon, G. Fantozzi, Subcritical crack propagation in 3Y-TZP ceramics: static and cyclic fatigue, J. Am. Ceram. Soc. 82 (1999) 3129–38.

[43] A. Shyam, E. Lara-Curzio, The double-torsion testing technique for determination of fracture toughness and slow crack growth behavior of materials: A review. J Mater Sci. 41 (2006) 4093–4104.

[44] D.P. Williams & A. G. Evans, A simple method for studying slow crack growth, J Test Eval. 1, (1973) 264-70.

[45] J. Chevalier, J. M. Drouin, and B. Cales, Bioceramics, 10, (1997) 135–138.

[46] W. Weibull, A statistical distribution function of wide applicability, J. Appl. Mech. 18 (1951) 293-305.

[47] IJ. Davies. Unbiased estimation of Weibull modulus using linear least squares analysis—A systematic approach. J. Eur. Ceram. Soc. 37 (2017) 369–380.

[48] T. Kosmac, C. Oblak, P. Jevnikar, N. Funduk, L. Marion, Strength and reliability of surface treated YTZP dental ceramics. J. Biomed. Mater. Res. 53 (4) (2000) 304-313.

[49] M. Saadaoui, C. Olagnon, G. Fantozzi, Influence of precracking procedure, environment, temperature and microstructure on R-curve behavior of alumina and PSZ ceramics. J. Eur. Ceram. Soc. 12 (5) (1993) 361–8.

[50] E. Apel, C. Ritzberger, N. Courtois, H. Reveron, J. Chevalier, M. Schweiger, F. Rothbrust, VM Rheinberger, W. Höland, Introduction to a tough, strong and stable Ce-TZP/MgAl2O4 composite for biomedical applications, J. Eur. Ceram. Soc. 32 (11) (2012) 2697-2703.

[51] B. Lawn, Fracture of Brittle Solids, second edition, Cambridge University Press, Cambridge, 1993.

[52] AH. De Aza, J. Chevalier, G. Fantozzi, M. Schehl, R. Torrecillas, Crack growth resistance of alumina, zirconia, and zirconia toughened alumina ceramics for joint prostheses, Biomaterials, 23 (3) (2002) 937-45.

[53] H. El Attaoui, M. Saadaoui, J. Chevalier, G. Fantozzi. Crack Propagation Behavior of Alumina with Different Grain Sizes under Static and Cyclic Fatigue, Key Eng. Mater. Vols. 317-318 (2006) 449-452.

[54] F. Zhang, J. Chevalier, C. Olagnon, B. Van Meerbeek, J. Vleugels, Slow crack growth and hydrothermal aging stability of an alumina-toughened zirconia composite made from La2O3-doped 2Y-TZP, J. Eur. Ceram. Soc. 37 (4) (2017) 1865–1871.

[55] S.M. Wiederhorn. Subcritical crack growth in ceramics. Fract Mech Ceram. (1974) 613–46. https://doi.org/10.1007/978-1-4615-7014-1_12.

[56] I. Touaiher, M. Saadaoui, J. Chevalier, H. Reveron, Effect of loading configuration on strength values in a highly transformable zirconia-based composite, Dent. Mater. 32 (2016) 211–219. https://doi.org/10.1016/j.dental.2016.06.023

[57] F. Kern, H. Reveron, J. Chevalier, R. Gadow, Mechanical behaviour of extremely tough tzp bioceramics, J. Mech. Behav. Biomed. Mater. 90 (2019) 395–403. https://doi.org/10.1016/j.jmbbm.2018.11.001.

[58] A. Liens, H. Reveron, T. Douillard, N. Blanchard, V. Lughi, V. Sergo, et al. Phase transformation induces plasticity with negligible damage in ceria-stabilized zirconia-based ceramics. Acta Mater, 183 (2020) 261–73, http://dx.doi.org/10.1016/j.actamat.2019.10.046.

[59] R.M. McMeeking, A.G. Evans, Mechanics of transformation-toughening in brittle materials. J. Am. Ceram. Soc. 65 (1982) 242–7.

[60] T. Kosmac, R. Wagner, N. Claussen, X-Ray determination of transformation depths in ceramics containing tetragonal ZrO2, J. Am. Ceram. Soc. 64 (1981) C-72-C-73.

[61] F. Zhang, J. Chevalier, C. Olagnon, S. Huang, W. Veulemans, K. Vanmeensel, J. Vleugels, Slow crack growth resistance of electrically conductive zirconia-based composites with non-oxide reinforcements, J. Eur. Ceram. Soc. 39 (2019) 641–646.

[62] K. Yoshida, F. Wakai, N. Nishiyama et al. Large increase in fracture resistance of stishovite with crack extension less than one micrometer. Sci Rep 5, (2015) 10993. https://doi.org/10.1038/srep10993.

[63] W.J. Xue, Z.P. Xie, G.W. Liu, W. Liu, J. Yi, R-curve behavior of 3Y-TZP at cryogenic temperatures, J. Am. Ceram. Soc. 94 (2011) 2775–2778.

[64] J. Chevalier, C. Olagnon, G. Fantozzi, Crack propagation and fatigue in zirconia-based composites, Composites Part A: Applied Science and Manufacturing 30(4) (1999) 525-530.

[65] M.E. Ebrahimi, J. Chevalier, G. Fantozzi, Slow crack-growth behavior of alumina ceramics, J. Mater. Res. 15 (1) (2000) 142–147.

[66] M.V. Swain, L.R.F. Rose, Strength limitations of transformation-toughened zirconia alloys, J. Am. Ceram. Soc. 69 (1986) 511–518.

[67] MF. Ashby, Materials selection in mechanical design, 3rd edn. Waltham, MA: Butterworth-Heinemann, 2005.

[68] S.R. Jansen, A.J.A. Winnubst, Y.J. He, H. Verweij, P. G. Th van der Varst, G. de With, Effects of grain size and ceria addition on Ageing behavior and tribological properties of Y-TZP ceramics, J. Eur. Ceram. Soc. 18 (1998) 557-563

[69] A. Paul, B. Vaidhyanathan, J. Binner. Hydrothermal Aging Behavior of Nanocrystalline Y-TZP Ceramics. J. Am. Ceram. Soc. vol. 94, no 7, (2011) 2146–2152.

[70] H. Tsubakino, R. Nozato, M. Hamamoto, Effect of Alumina Addition on the Tetragonal-to-Monoclinic Phase Transformation in Zirconia- 3 mol% Yttria, J. Am. Ceram. Soc. vol. 74, no 2, (1991) 440–443.

Tables captions:

Table 1: Properties of some Y-TZP ceramics with % mole Y_2O_3 < 3 compared to standard 3Y-TZP.

Figures captions:

Figure 1: SEM micrographs of polished and thermally treated surface.

Figure 2: Examples of stress-displacement curves obtained during 4PB and 3B3B tests.

Figure 3: Optical micrographs (Nomarski contrast) of transformation zones observed at the tensile side of 3B3B and 4PB samples for applied loads respectively of 1560 MPa and 890 MPa. In 4PB, the position of parallel transformation bands are indicated by arrows; randomly distributed scratches are here observed are related to the initial surface state of the samples.

Figure 4: Strength distribution obtained with the 4BP test on 30 specimens and best fit to a Weibull distribution (Weibull modulus of 16 and characteristic strength of 1029 MPa) or a Normal distribution. (mean strength σ_f = 995 MPa and standard deviation of 77 MPa).

Figure 5: Crack growth resistance curve.

Figure 6: *V*-K_I diagram of the investigated material (blue symbols) compared to 3Y-TZP [40] and a 10Ce-TZP/$MgAl_2O_4$ composite [50]. For 1.5Y-TZP solid symbols correspond to relaxation test and circles to constant loading tests. The indicated fracture toughness (K_{IC} = 10.6 MPa$\sqrt{m}$) corresponds to the value measured separately from DT fast loading tests.

Figure 7: Evolution of the impact-induced transformation zone size with the kinetic energy of the drop ball.

Figure 8: 3D confocal images of the transformation zones developed under impact testing with drop heights of 30 and 45 cm (corresponding respectively to kinetic energies of $7.7x10^{-2}$ and $11.7x10^{-2}$ J) and their radial topography profile curves as a function of the radial distance, *r*.

Figure 9: Aging kinetics of the present 1.5Y-TZP at 134°C, 2 bars, compared to a standard 3Y-TZP [40].

Figure 10: XRD patterns of fractured and polished surfaces.

Figure 11: 3D confocal image around a crack after a SEVNB test with an illustration of a roughness profile.

Figure 12: Normalized *V*-K_I/K_{IC} diagram for 1.5Y-TZP, 3Y-TZP [40] and 10Ce-TZP/$MgAl_2O_4$ composite [50].

Figure 13: Ashby plot of fracture toughness vs strength. The diagonal lines correspond to the process-zone size, d, in mm. The studied 1.5Y-TZP material is between standard 3Y-TZP [40] and Ce-TZP-Alumina-Aluminates composites presenting transformation-induced plasticity [22].

Table 1: Properties of some Y-TZP ceramics with % mole Y_2O_3 < 3 compared to standard 3Y-TZP.

% mol Y_2O_3	Grain size (nm)	Toughness (MPa$\sqrt{m}$)	Strength (MPa)	References
1	90	16 -17 IF	-	25
1.5	110	16 -17 IF		25
	85	7.9 CNB 15.5 IF	-	15
	320	16 IF	1980 3PB	26
	200-600	6 IF	300 3PB	27
	-	12.6 - 14.8 IF	-	13
2	-	11.9 - 13.9 IF	-	13
	250	5.7 IF	-	28
	150 -900	3.1- 4.3*	-	9
	500	5 ISB	-	7
	429	5.9 IF	-	29
	597	6.4 SEVNB	994 3PB	14
	555	5.3 SEVNB	817 3PB	14
	200-600	16 IF	1500 3PB	27
	290	8.6 DT	-	30
2.5	230	5.1 DT	-	30
	200-600	6 IF	1600 3PB	27
	300	4.3 IF	1076 3PB	31
	300	4.2 *	-	32
2.6 - 2.85	160-190	10.5 - 12.5 ISB	900 – 1050 4PB	16
3	< 1	4 - 6 SEVNB	900 - 1200 4PB	4 - 6

ISB: Indentation Strength in Bending ** Plateau of the R-curve*
4PB: Four Points Bending *IF: Indentation Fracture*
3PB: Three Points Bending *SEVNB: Single-edge V-notched Beam*
CNB: Chevron Notched Beam *DT: Double Torsion*

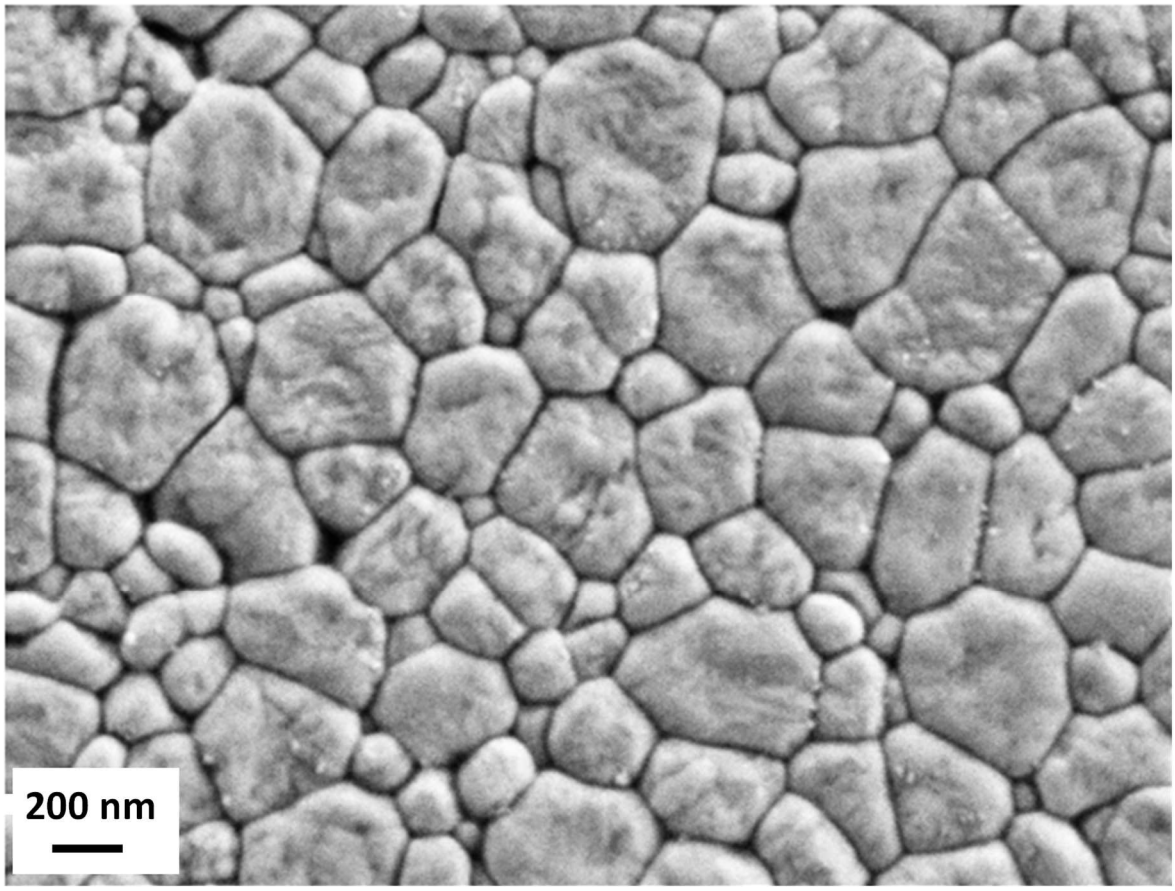

Figure 1: SEM micrographs of polished and thermally treated surface.

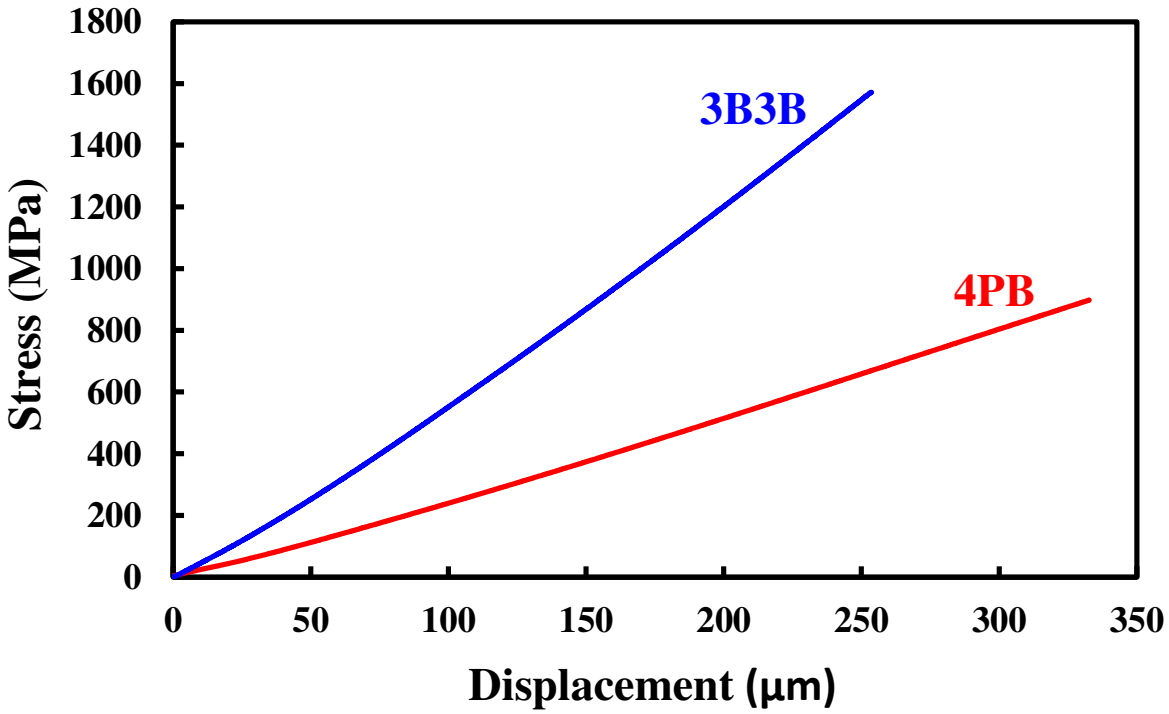

Figure 2: Examples of stress-displacement curves obtained during 4PB and 3B3B tests.

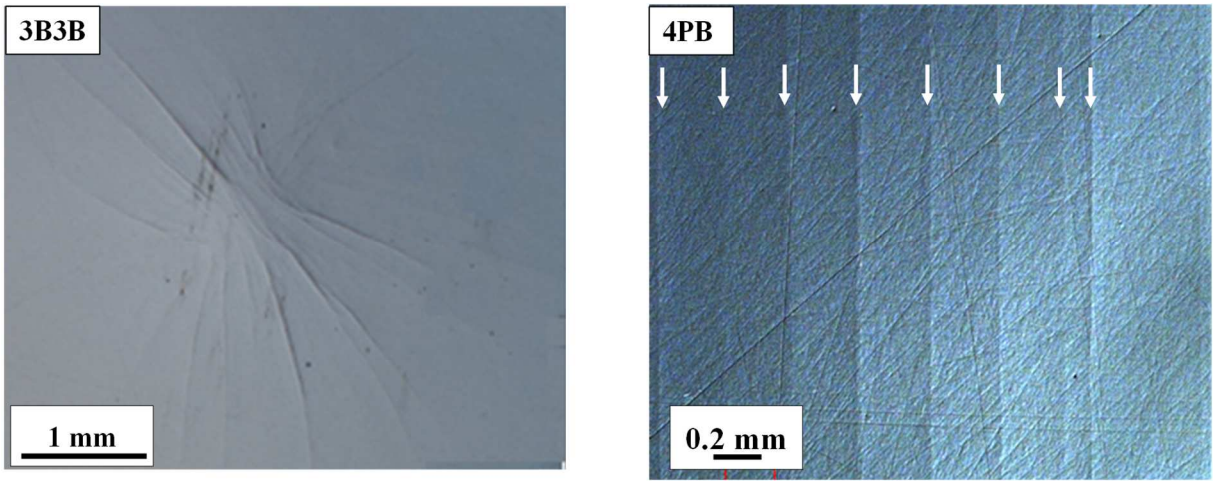

Figure 3: Optical micrographs (Nomarski contrast) of transformation zones observed at the tensile side of 3B3B and 4PB samples for applied loads respectively of 1560 MPa and 890 MPa. In 4PB, the position of parallel transformation bands are indicated by arrows; randomly distributed scratches are here observed are related to the initial surface state of the samples**.**

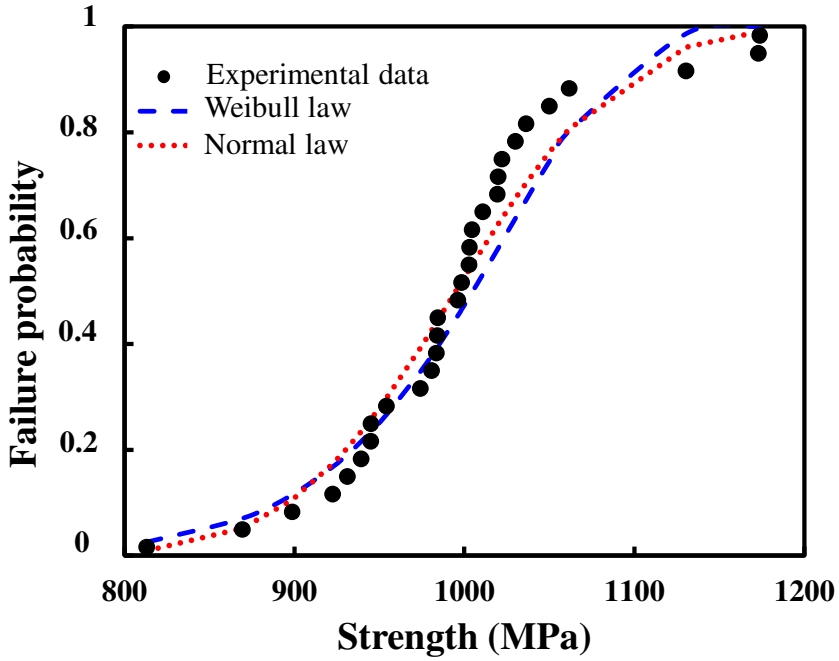

Figure 4: Strength distribution obtained with the 4BP test on 30 specimens and best fit to a Weibull distribution (Weibull modulus of 16 and characteristic strength of 1029 MPa) or a Normal distribution. (mean strength σ_f = 995 MPa and standard deviation of 77 MPa).

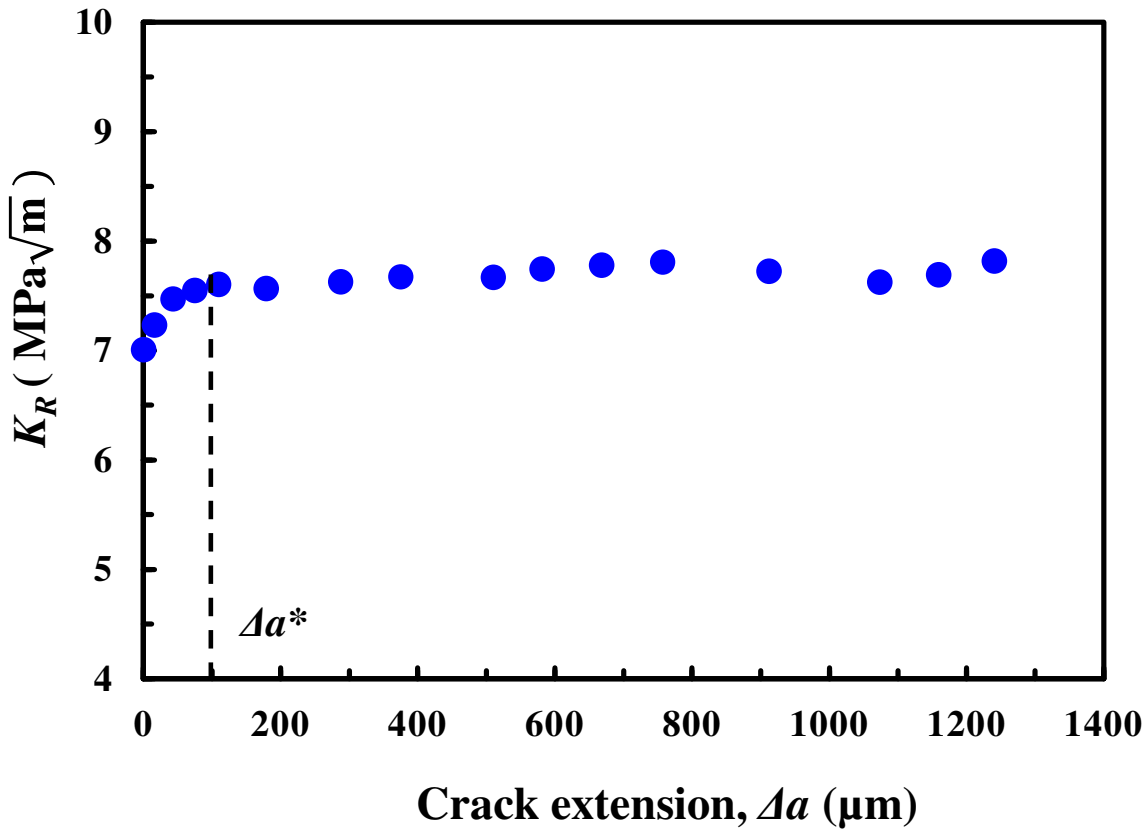

Figure 5: Crack growth resistance curve.

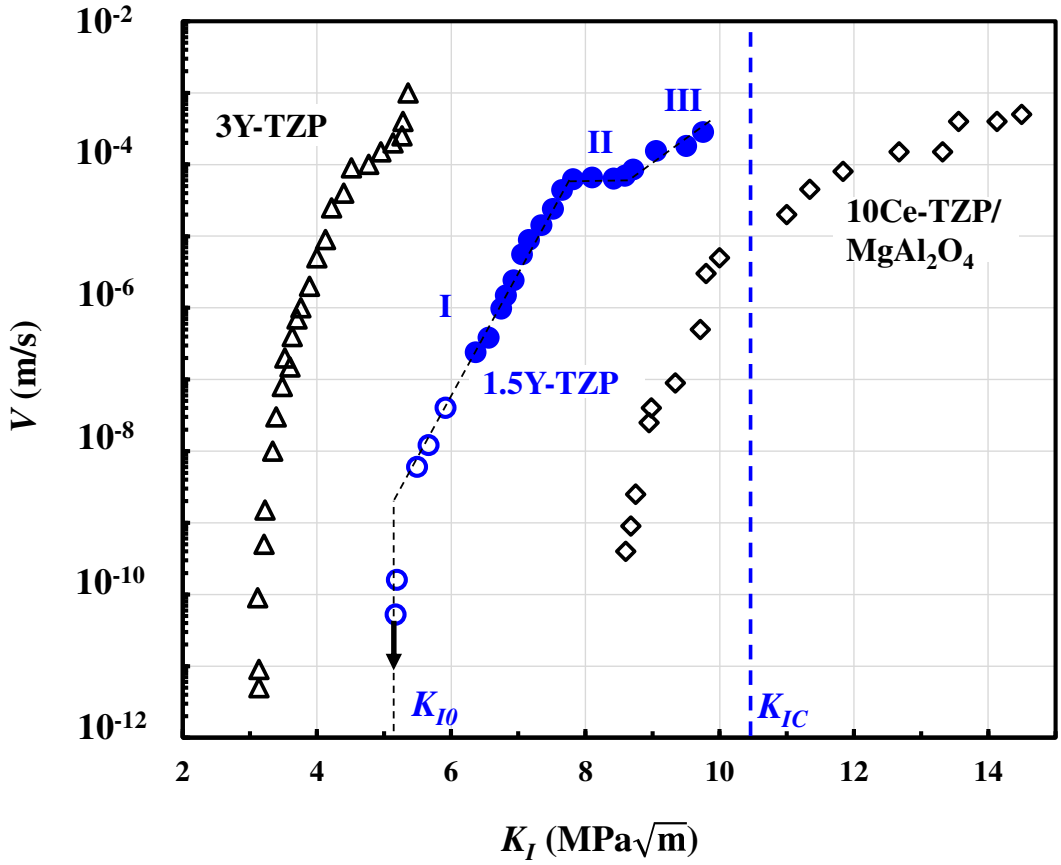

Figure 6: V-K_I diagram of the investigated material (blue symbols) compared to 3Y-TZP [40] and a 10Ce-TZP/$MgAl_2O_4$ composite [50]. For 1.5Y-TZP solid symbols correspond to relaxation test and circles to constant loading tests. The indicated fracture toughness (K_{IC} = 10.6 MPa$\sqrt{m}$) corresponds to the value measured separately from DT fast loading tests.

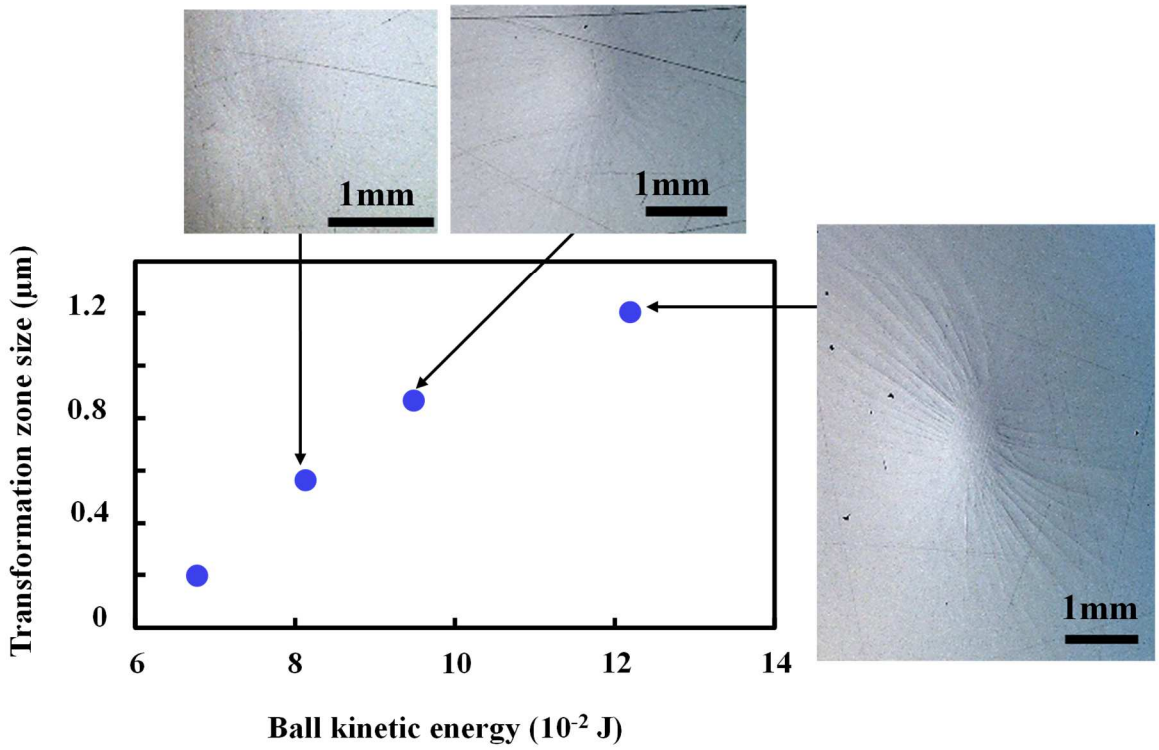

Figure 7: Evolution of the impact-induced transformation zone size with the kinetic energy of the drop ball.

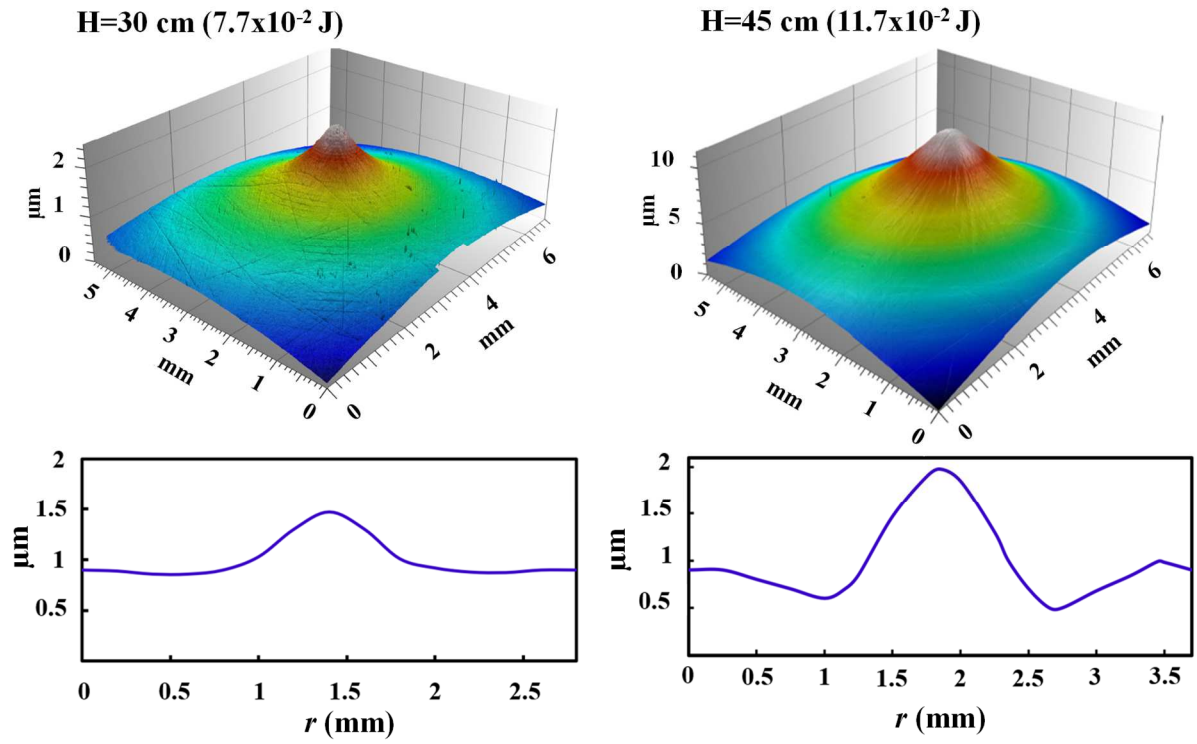

Figure 8: 3D confocal images of the transformation zones developed under impact testing with drop heights of 30 and 45 cm (corresponding respectively to kinetic energies of 7.7×10^{-2} and 11.7×10^{-2} J) and their radial topography profile curves as a function of the radial distance, *r*.

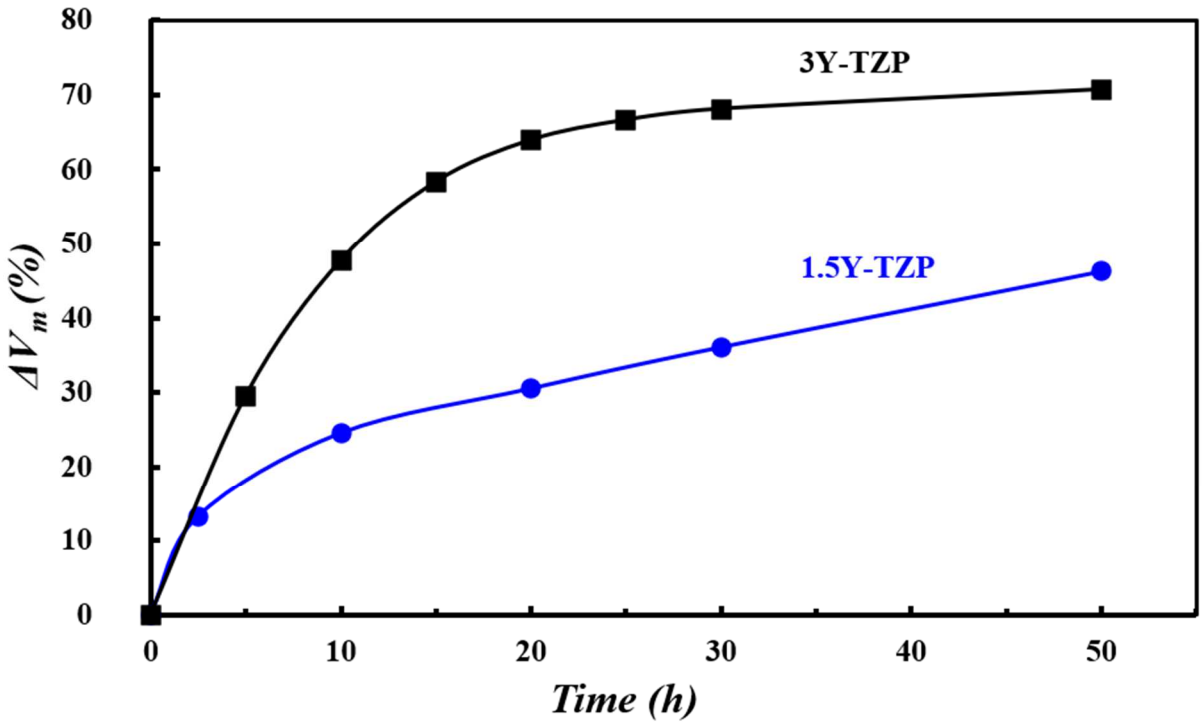

Figure 9: Aging kinetics of the present 1.5Y-TZP at 134°C, 2 bars, compared to a standard 3Y-TZP [40].

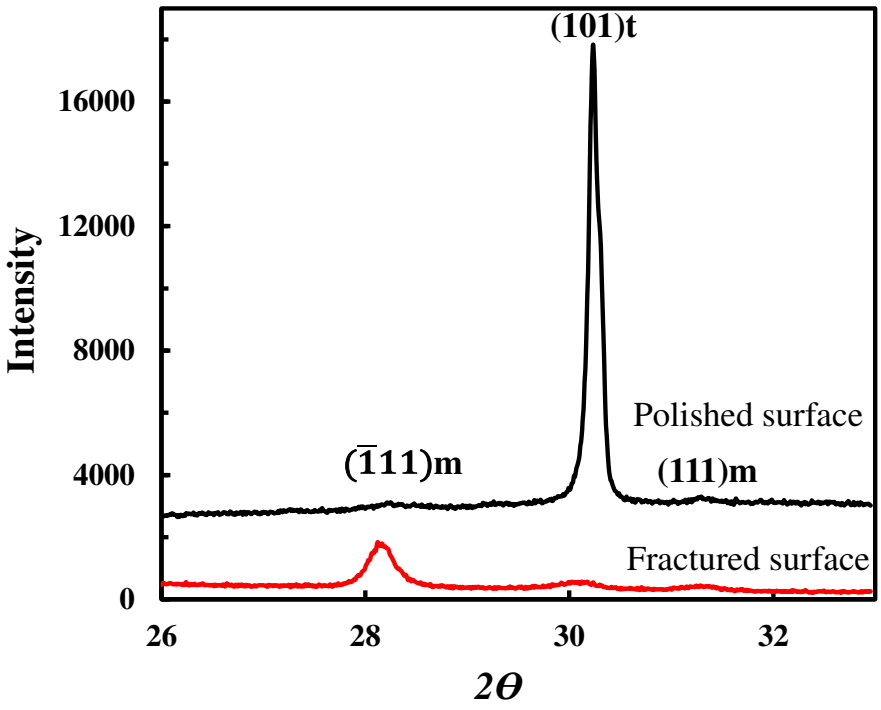

Figure 10: XRD patterns of fractured and polished surfaces.

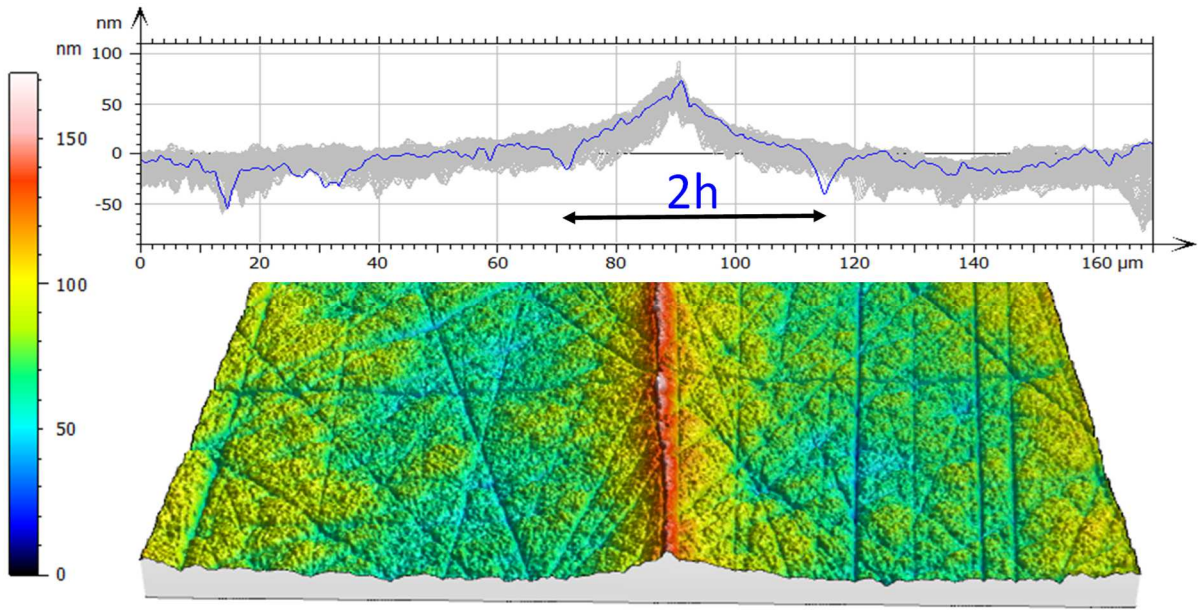

Figure 11: 3D confocal image around a crack after a SEVNB test with an illustration of a roughness profile.

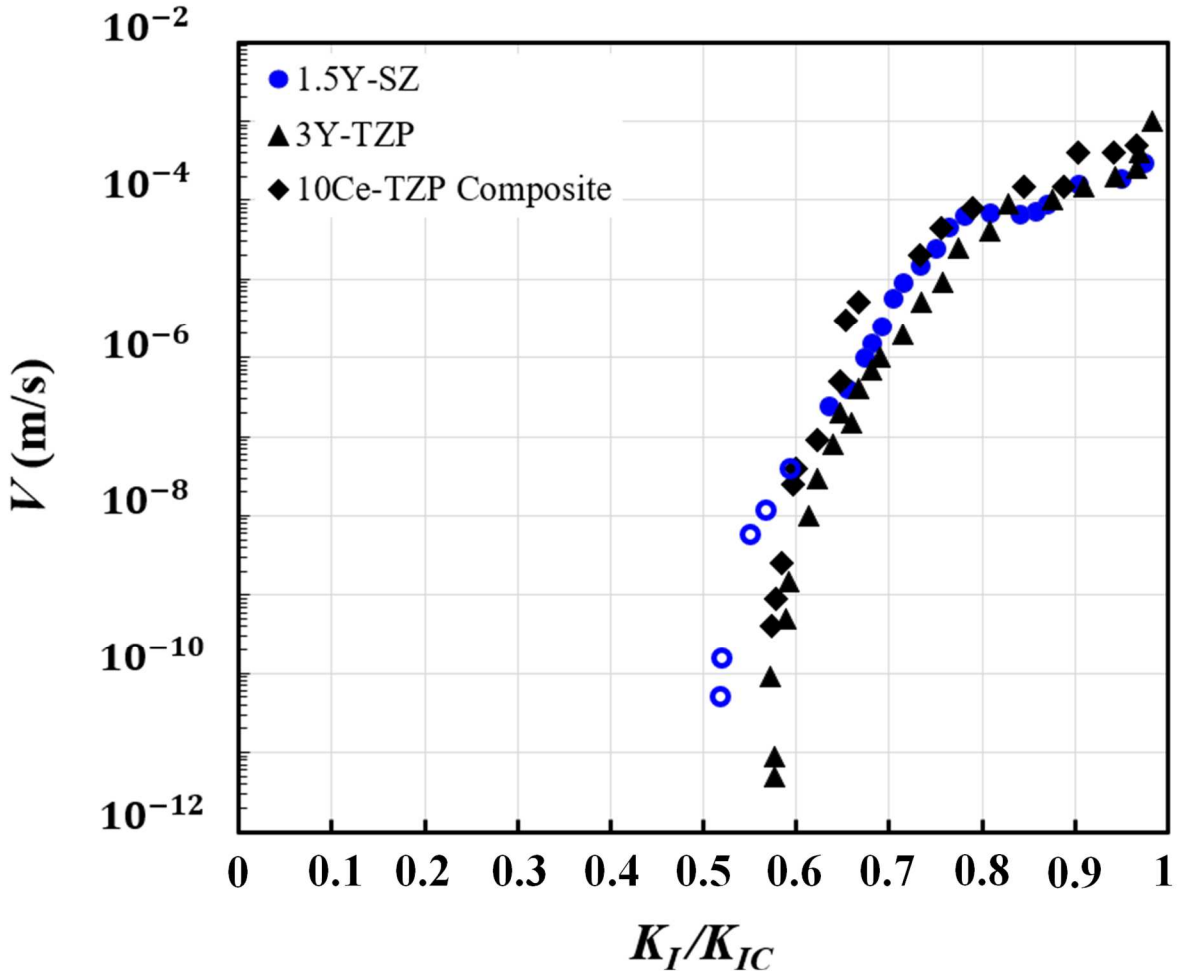

Figure 12: Normalized V-K_I/K_{IC} diagram for 1.5Y-TZP, 3Y-TZP [40] and 10Ce-TZP/$MgAl_2O_4$ composite [50].

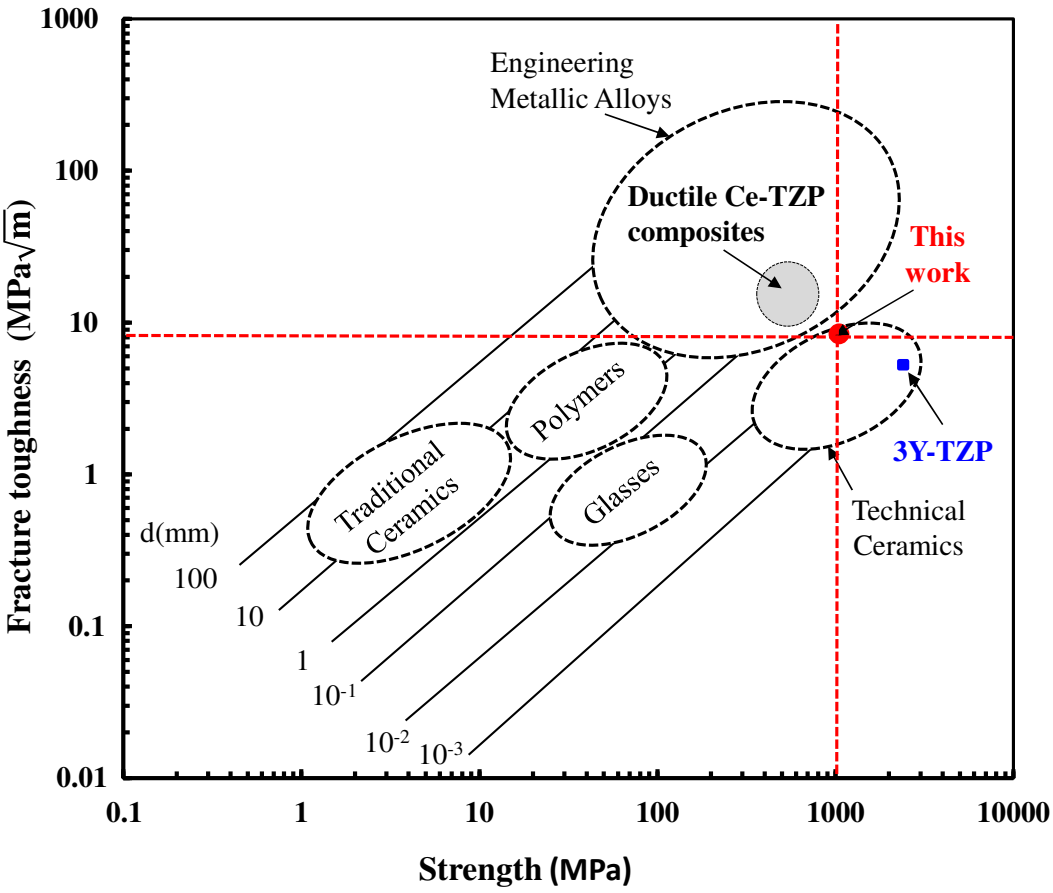

Figure 13: Ashby plot of fracture toughness vs strength. The diagonal lines correspond to the process-zone size, d, in mm. The studied 1.5Y-TZP material is between standard 3Y-TZP [40] and Ce-TZP-Alumina-Aluminates composites presenting transformation-induced plasticity [22].